Density-functional theory study of the effect of pressure on the elastic properties of CaB_6

Han Han(韩 晗)†

Surface Physics Laboratory (National Key Laboratory), Key Laboratory of Computational Physical Sciences, and Department of Physics, Fudan University, Shanghai 200433, *China*

(Received 15 January 2013; revised manuscript received 27 February 2013)

Under high pressure, the long believed single-phase material CaB_6 was latterly discovered to have a new phase tI56. Based on the density-functional theory, the pressure effects on the structural and elastic properties of CaB_6 are obtained. The calculated bulk, shear, and Young's moduli of the recently synthesized high pressure phase tI56-CaB_6 are larger than those of the low pressure phase. Moreover, the high pressure phase of CaB_6 has ductile behaviors, and its ductility increases with the increase of pressure. On the contrary, the calculated results indicate that the low pressure phase of CaB_6 is brittle. The calculated Debye temperature indicates that the thermal conductivity of CaB_6 is not very good. Furthermore, based on the Christoffel equation, the slowness surface of the acoustic waves is obtained.

Keywords: density-functional theory, elastic properties, pressure effects, acoustic properties

PACS: 71.15.Mb, 62.20.D–, 71.20.Ps **DOI:** 10.1088/1674-1056/22/7/077101

1. Introduction

Pressure has a great effect on the properties of a material. Under high pressure, some materials only change their lattice parameters without changing their basic atomic network, while some other materials exhibit surprising structural changes.[1–7] CaB_6 is a member of the MB_6 (M = metal element) family, which is known for a range of properties and applications, such as thermionic emitters and superconductors.[8–10] For a long time, only the cubic crystal structure (cP7) was found in MB_6 family materials. Until recently, a new structure (tI56) of CaB_6 under high pressure was found by Kolmogorov *et al.*[11] We adopt density-functional theory (DFT) to study the structural and elastic properties of different CaB_6 phases under different pressures.

2. Calculation methods

Our calculations are performed under the framework of DFT as implemented in the ABINIT package.[12] Exchange and correlation effects are treated by the generalized gradient approximation (GGA).[13] Electron–ion interactions are described by the norm-conserving pseudopotentials,[14,15] and the wave functions are expanded in a plane-wave basis set with an energy cutoff of 80 Ry. The k-points in the Brillouin zone (BZ) of the primitive unit cell are sampled on a $12\times12\times12$ mesh for a cubic phase and on a $6\times6\times6$ mesh for tetragonal phase. The equilibrium structure is obtained by optimizing atomic positions until the forces on the atoms are less than 5 meV/Å. The elastic constants are calculated within the framework of density-functional perturbation theory (DFPT).[16]

3. Results and discussion

3.1. Atomic structure and bonding properties

The CaB_6 crystal under a low pressure has a cubic structure, which is analogous with CsCl. The [B_6] group occupies the positions of the Cl cation; the position of Ca is similar to that of Cs. When the pressure is larger than 32 GPa, the structure of CaB_6 transfers to the tI56 phase, whose unit cell contains as many as 56 atoms. The primitive unit cells of CaB_6 in cP7 and tI56 phases are given in Figs. 1(a) and 1(b), respectively. In order to compare with the experimental values, the calculated lattice constants of the tI56 phase under 43.8 GPa are listed in Table 1. The calculated volume with the Perdew–Burke–Ernzerhof (PBE) functional[17] is 402.0 Å^3, which agrees well with the experimental value 408.4 Å^3. However, the calculated volume with the local density approximation (LDA) functional[18] is 388.1 Å^3, which is much smaller than the experimental value. Therefore, the PBE functional is adopted for further calculations.

The crystal structures of cubic and tetragonal CaB_6 are optimized without pressure and are listed in Table 2. In the cP7-CaB_6 phase, a calcium has 24 nearest-neighbor boron atoms. The Ca–B bond length is 3.051 Å, and the B–B bond length is 1.750 Å. When it comes to the tI56-CaB_6 phase, there are two inequivalent Ca cations in the unit cell. The coordination number for calcium cation is 20, and the Ca–B bond lengths vary from 2.644 Å to 2.807 Å. In addition, the B–B bond lengths vary from 1.647 Å to 2.104 Å. The Ca–B bond lengths of the tI56-CaB_6 phase are much shorter than those of cP7-CaB_6. Therefore, the tI56-CaB_6 phase has a more compact structure and a higher density than the cP7-CaB_6 phase.

†Corresponding author. E-mail: fdu.hhan@gmail.com

© 2013 Chinese Physical Society and IOP Publishing Ltd

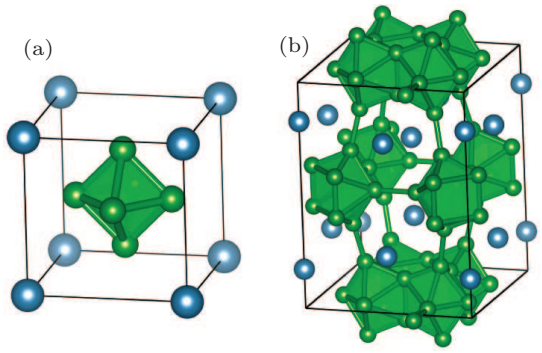


Fig. 1. (color online) Crystal structures of CaB_6 under different pressures. The blue and green spheres are Ca and B atoms, respectively. The B octahedra are shown in green. (a) The cubic low-pressure phase of CaB_6 (cP7 in Pearson notation, space group Pm-$3m$). (b) The tetragonal high-pressure phase of CaB_6 (tI56 in Pearson notation, space group $I4/mmm$).

Table 1. Calculated lattice constants and volume of the conventional cell of CaB_6 in tI56 phase at 43.8 GPa, where Δa and Δc are the relative errors of calculated lattice constants compared with the experimental data.

	$(a=b)$/Å	c/Å	Volume/Å^3	Δa/%	Δc/%
Expt.[11]	6.779	8.887	408.4		
LDA	6.656	8.760	388.1	–1.81	–1.43
PBE	6.735	8.862	402.0	–0.65	–0.28

In order to reveal the bonding properties of CaB_6, the differences between the crystal charge and the atomic charge are depicted in Fig. 2. The positive value mainly locates between boron atoms, which indicates the robust covalent binding between boron atoms. Since cP7-CaB_6 is made out of boron octahedra, these boron atoms form B-squares in the (001) plane (Fig. 2(a)). One can see that the electron charge densities on the B–B bond, which bridge neighbor B-squares, are higher than those on the bonds in the B-squares. The reason is that the former bond length is smaller (1.67 Å) than the latter (1.75 Å). As depicted in Fig. 2(b), the boron atoms in tI56-CaB_6 form octagons in the (001) plane. Since the bond length between B atoms alone the (010) direction (1.68 Å) is smaller than that alone the (110) direction (1.75 Å), the charge densities of the former are higher than those of the latter. There is ionic bonding between Ca^{2+} and B_6^{2-} polymeric anion in the cP7-CaB_6 phase.[19] Based on the Bader charge analysis,[20–23] the ionic formulas of the cP-CaB_6 and tI56-CaB_6 phases are $Ca^{+1.53}(B_6)^{-1.53}$ and $Ca^{+1.34}(B_6)^{-1.34}$, respectively. Additionally, CaB_6 is a member of the large MB_6 family, which has an ionic interaction between the metal cation M and the anionic group B_6.[24–26] Therefore, there is ionic bonding between the B group and Ca in both phases.

Table 2. Calculated atomic positions for CaB_6 with symmetries Pm-$3m$ and $I4/mmm$ by PBE functional without pressure, where WP refers to the Wyckoff position.

Phase	$(a=b)$/Å	c/Å	Atom	WP	Multiplicity	x	y	z
cP7	4.149	4.149	B	f	6	0.2017	0.5000	0.5000
(Pm-$3m$)			Ca	a	1	0.0000	0.0000	0.0000
tI56	7.151	9.363	B	l	16	–0.3024	0.1252	0.0000
($I4/mmm$)			B	m	16	–0.2230	–0.223	0.3400
			B	n	16	0.0000	0.2081	0.4120
			Ca	e	4	0.0000	0.0000	0.2500
			Ca	d	4	0.0000	0.5000	0.2500

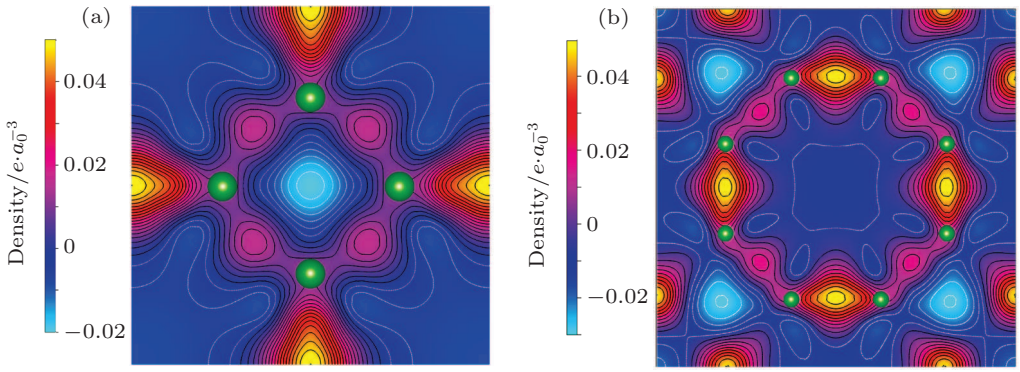


Fig. 2. (color online) Deformation charge density (difference between the crystal charge and the atomic charge) of CaB_6 in cP7 phase at 0 GPa (a) and tI56 phase at 43.8 GPa (b) in the (100) plane (see Fig. 1). The boron atoms (the green spheres) in the plane are plotted out. Contours are added with intervals $0.003e/a_0^3$ and $0.005e/a_0^3$ for panels (a) and (b), respectively, where e is the electron charge, and a_0 is the Bohr radius. Contours with black (white) lines indicate positive (negative) values.

3.2. Elasticity-relevant properties

The elastic constants describe the response of a material to an externally applied stress.[27] Additionally, the mechanical stability and stiffness of the material are closely related with the elastic constants. Cubic crystal structures have three independent elastic constants C_{11}, C_{12}, and C_{44}. Tetragonal crystal structures have six independent elastic constants C_{11}, C_{12}, C_{13}, C_{33}, C_{44}, and C_{66}. The calculated elastic constants under different pressures for CaB_6 are plotted in Fig. 3. For both phases of cP7 and tI56, C_{11} increases more quickly than the other elastic constants with the increase of pressure. The C_{44} of cP7 is larger than that of tI56 by 100–200 GPa, which makes the elastic properties of these two phases differ a lot as we discuss next. The mechanical stability criterion reflects the structural stability of a material.[28] The criterion for a cubic crystal is given as

$$C_{11} > 0, \quad C_{44} > 0, \quad C_{11} > |C_{12}|, \quad (C_{11} + 2C_{12}) > 0. \quad (1)$$

While for a tetragonal crystal, it is given as[29]

$$\begin{aligned} &C_{11} > 0, \quad C_{33} > 0, \quad C_{44} > 0, \quad C_{66} > 0, \\ &C_{11} - C_{12} > 0, \\ &C_{11} + C_{33} - 2C_{13} > 0, \\ &2(C_{11} + C_{12}) + C_{33} + 4C_{13} > 0. \end{aligned} \quad (2)$$

The calculated elastic constants for both phases under different pressures satisfy the criteria, which means that these two phases are stable.

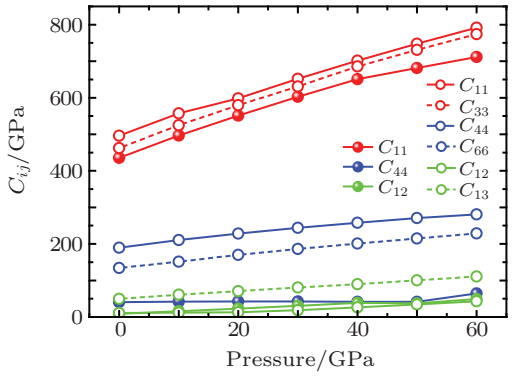


Fig. 3. (color online) Calculated pressure dependences of elastic constants for CaB_6 in cP7 (solid circles) and tI56 (open circles).

Based on the elastic constants, we deduce the bulk modulus, shear modulus, Young's modulus, and Poisson ratio, which are widely used to describe the mechanical behaviors of materials. The Voigt and the Reuss approximations[30–32] are widely used to estimate the bulk and the shear moduli.[33–35] Within the Voigt approximation, the general expressions of bulk and shear moduli are

$$B_V = [(C_{11} + C_{22} + C_{33}) + 2(C_{12} + C_{13} + C_{23})]/9, \quad (3)$$

$$G_V = [(C_{11} + C_{22} + C_{33}) - (C_{12} + C_{13} + C_{23}) + 3(C_{44} + C_{55} + C_{66})]/15. \quad (4)$$

While with the Reuss approximation, they are

$$B_R = 1/[(S_{11} + S_{22} + S_{33}) + 2(S_{12} + S_{13} + S_{23})], \quad (5)$$

$$G_R = 15/[4(S_{11} + S_{22} + S_{33}) - 4(S_{12} + S_{13} + S_{23}) + 3(S_{44} + S_{55} + S_{66})], \quad (6)$$

where S_{ij} are the components of the elastic compliance matrix, which is the inverse of matrix C_{ij}.

It is found that CaB_6 has a tetragonal structure under a high pressure. For this tetragonal phase, the shear and bulk moduli are obtained using the following equations:

$$B_V = [2(C_{11} + C_{12}) + C_{33} + 4C_{13}]/9, \quad (7)$$

$$G_V = (M + 3C_{11} - 3C_{12} + 12C_{44} + 6C_{66})/30, \quad (8)$$

$$B_R = C^2/M, \quad (9)$$

$$G_R = 15/[18B_V/C^2 + 6/(C_{11} - C_{12}) + 6/C_{44} + 3/C_{66}], \quad (10)$$

$$C^2 = (C_{11} + C_{12})C_{33} - 2C_{13}^2,$$

$$M = C_{11} + C_{12} + 2C_{33} - 4C_{13}. \quad (11)$$

For cubic systems, we have $C_{66} = C_{44}$, $C_{33} = C_{11}$, $C_{13} = C_{12}$. Applying these conditions to Eqs. (7)–(11), we obtain

$$B_V = B_R = (C_{11} + 2C_{12})/3, \quad (12)$$

$$G_V = (C_{11} - C_{12} + 3C_{44})/5, \quad (13)$$

$$G_R = \frac{5(C_{11} - C_{12})C_{44}}{4C_{44} + 3(C_{11} - C_{12})}. \quad (14)$$

Within the Voigt–Reuss–Hill approximation, bulk modulus B and shear modulus G are represented as

$$B = (B_V + B_R)/2, \quad G = (G_V + G_R)/2. \quad (15)$$

Then Young's modulus E and Poisson ratio v can be obtained by

$$E = 9BG/(3B + G), \quad v = (3B - 2G)/(6B + 2G). \quad (16)$$

The calculated relevant results are shown in Fig. 4. The velocities of the transverse (V_t), longitudinal (V_l) acoustic waves and the average velocity (V_a) are obtained by[36,37]

$$V_l = \sqrt{(3B + 4G)/3\rho},$$

$$V_t = \sqrt{G/\rho}, \quad V_a = \left[\frac{1}{3}\left(\frac{2}{V_t^3} + \frac{1}{V_l^3}\right)\right]^{-1/3}. \quad (17)$$

Finally, the Debye temperature Θ_D can be obtained by

$$\Theta_D = \frac{h}{k_B}\left[\frac{3n}{4\pi}\left(\frac{N_A\rho}{m}\right)\right]^{1/3} V_a, \quad (18)$$

where h is the Planck constant, k_B is the Boltzmann constant, n is the number of atoms in the formula unit, N_A is the Avogadro number, ρ is the density of the crystal, and m is the molecular weight.

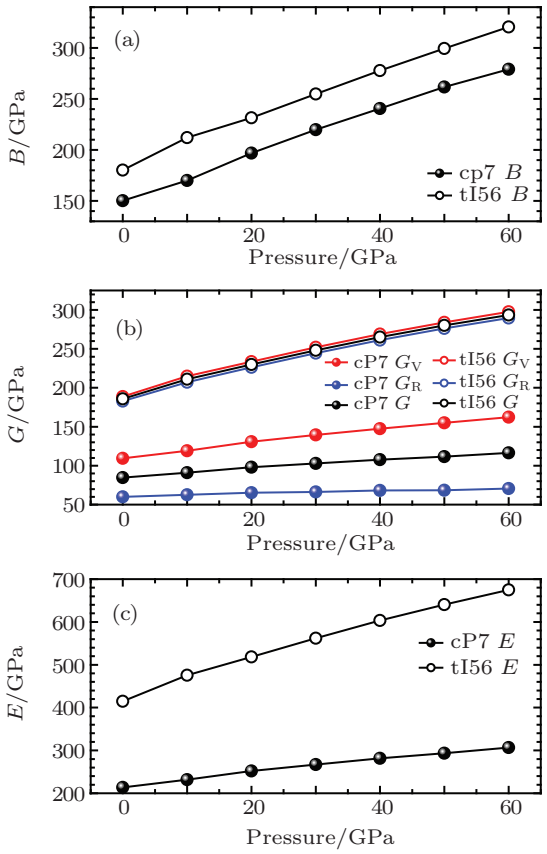


Fig. 4. (color online) Pressure dependences of (a) bulk modulus B and (b) shear modulus G within the Voigt and Reuss approximations and (c) Young's moduli E for cP7 (solid circles) and tI56 (open circles) CaB_6.

The bulk modulus reflects the resistance of a material to a volume change and its response to a hydrostatic pressure.[33] The shear modulus describes the resistance of a material to a shape change. The bulk and shear moduli increase with the increase of pressure. This is because the B–B bond length decreases and the B–B interaction increases with the increase of pressure. The calculated bulk moduli of cP7-CaB_6 and tI56-CaB_6 under different pressures are all above 150 GPa, which are comparable to those of classic hard materials, such as β-B_2O_3 (169.9 GPa)[38] and α-Al_2O_3 (253.7 GPa).[39] Therefore, cP7-CaB_6 and tI56-CaB_6 are hard materials.

For the application of materials, the brittle or ductile behavior is of great importance. Pugh proposed that the bulk modulus is associated with the resistance to fracture, while the shear modulus is associated with the resistance to plastic deformation.[40] Bulk modulus B and shear modulus G for tI56-CaB_6 are very close. In contrast, for cP7-CaB_6, the shear modulus is almost half of the bulk modulus. The ratio of bulk modulus to shear modulus (B/G) is frequently used to discriminate the brittle properties of materials.[40] According to the criterion given in Refs. [41]– [43], a material is brittle if B/G is less than 1.75. Otherwise, it behaves in a ductile manner. The relevant results are shown in Fig. 5(a). In the case of cP7-CaB_6, the B/G ratio increases from 1.77 to 2.40 when the pressure increases from 0 GPa to 60 GPa. This trend indicates that cP7-CaB_6 behaves in a ductile manner. On the contrary, the B/G ratio of tI57-CaB_6 is below 1.10, which indicates that tI56-CaB_6 behaves in a brittle manner. Therefore, the pressure induced phase transition can significantly change the brittle behavior of CaB_6. The ductility or brittleness can also be characterized by the Poisson ratio. The Poisson ratio is the ratio of transverse contraction strain to longitudinal extension strain under a stretching force. The Poisson ratio is smaller than 1/3 for brittle materials and bigger than 1/3 for ductile materials.[44] For tI56-CaB_6, the Poisson ratio is only 0.12–0.15, which also indicates that tI56-CaB_6 is brittle. Therefore, attention should be paid when CaB_6 is used under a high pressure.

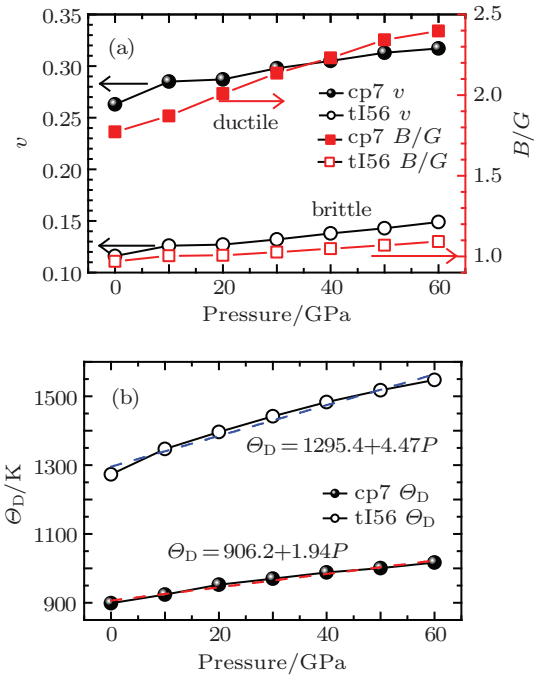


Fig. 5. (color online) Pressure dependences of (a) Poisson ratios v and (b) Debye temperature Θ_D for CaB_6 in cP7 and tI56 phases. The B/G ratio of tI56-CaB_6 is below 1.75, indicating a brittle material, while cP7-CaB_6 is not brittle. The linear fitted dotted lines are plotted in panel (b).

The Debye temperature is closely related to many physical properties of the material, such as specific heat, melting temperature, and thermal conductivity. At low temperature, the vibrational excitations arise solely from acoustic modes, and the Debye temperature calculated from the elastic constants is the same as that determined from the specific heat measurement. The calculated velocity of the longitudinal acoustic wave for cP7-CaB_6 is 10.4–11.8 km/s and that of the transverse acoustic wave is 5.9–6.1 km/s, giving the Debye temperature 899.0–1016.9 K. In contrast, for tI56-CaB_6, those values increase to 12.1–14.0 km/s, 8.0–9.0 km/s, and 1273.0–1547.3 K, respectively. Figure 5(b) shows that the Debye temperature increases linearly with increasing pressure (4.47 K/GPa for tI56-CaB_6 and 1.94 K/GPa for cP7-CaB_6). A high Debye temperature implies a high thermal

conductivity.[45] The Debye temperature of CaB_6 is much lower than that of diamond (around 2230 K). This indicates that the thermal conductivity of CaB_6 is not very good.

3.3. Acoustic properties

The ultrasonic wave velocity measurement is often used to determine the elastic constants.[46–49] In experiments, the ultrasonic wave velocities of certain directions can be measured and used to obtain the elastic constant with the Christoffel equation. The Christoffel equation is written as[50]

$$[l_{iK}c_{KL}l_{Lj} - \delta_{jk}\rho V^2][\alpha_j] = 0, \quad (j,k = 1,2,3), \qquad (19)$$

where c_{KL} is the elastic constants, l is the propagation matrix, δ_{jk} is the Kronercker sign, ρ is the density of the crystal, α_j is the eigenvector, and V is the velocity of the acoustic wave.

For a given direction, three velocities are determined by solving the Christoffel equation. By changing the propagation direction, we get the velocity as a function of the propagation direction. Usually, it is more convenient to use the slowness surface (the inverse of the velocity) in practice. We calculate the slowness curves of CaB_6 for both cP7 and tI56 phases in xy and yz planes and show them in Fig. 6 (for the cubic phase, yz plane is equivalent to xy plane). It can be found that there is a significant change in the acoustic properties of CaB_6 when the phase transition happens. There are three acoustic waves in each direction: quasi-longitudinal, quasi-transverse, and pure transverse modes. It can be found that the velocities of the quasi-longitudinal mode are much larger than those of the other two. Taking an overall view, for both cP7-CaB_6 and tI56-CaB_6, the minimum value of the slowness surface is the longitudinal mode in the (100) direction, which indicates that the velocity is largest along this direction.

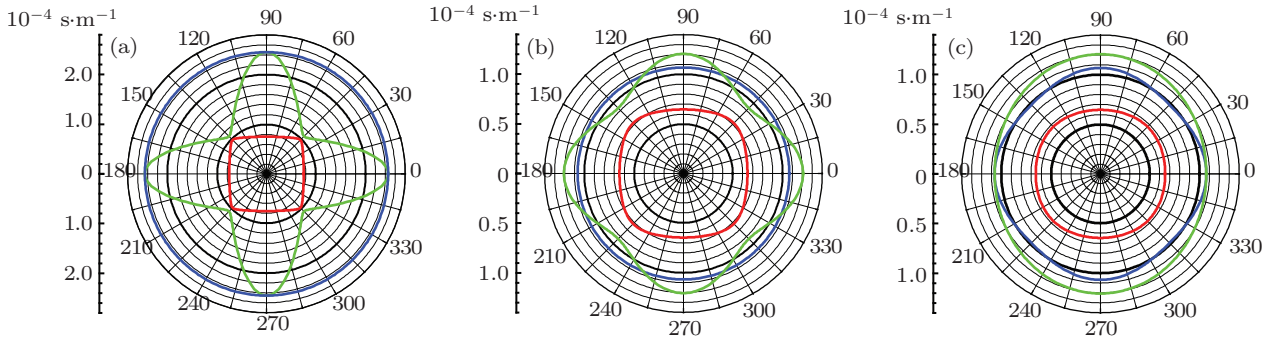


Fig. 6. (color online) Slowness curves of acoustic waves of CaB_6: (a) propagation in xy plane for cP7-CaB_6, (b) propagation in xy plane for tI56-CaB_6, and (c) propagation in yz plane for tI56-CaB_6. Red, green, and blue lines are quasi-longitudinal, quasi-transverse, and pure transverse modes, respectively.

4. Conclusion

In this work, we use the density functional theory to study the pressure effects on the atomic structure, elastic properties, and acoustic properties of CaB_6. Our calculated results show that the phase transition induced by pressure affects the materials' properties significantly. We find that the calculated bulk, shear, and Young's moduli of tI56-CaB_6 (high pressure phase) are larger than those of cP7-CaB_6 (low pressure phase). The reason is that the atoms in tI56-CaB_6 are closer and have stronger interactions than those in cP7-CaB_6. Furthermore, CaB_6 under low pressures has ductile behaviors, and its ductility increases with the increase of pressure. However, CaB_6 changes from a ductile material (cP7-CaB_6) to a brittle one (tI56-CaB_6) when the phase transition happens under a high pressure. Therefore, attention should be paid when CaB_6 is used under a high pressure. Besides, the calculated Debye temperature indicates that the thermal conductivity of CaB_6 is not very good. Based on the Christoffel equation, the slowness surface of acoustic waves of CaB_6 is calculated to describe its acoustic properties. These calculated results are a step forward to obtaining more comprehensive understanding of the properties of CaB_6.

References

[1] McMahon M I and Nelmes R J 2006 *Chem. Soc. Rev.* **35** 943
[2] Pickard C J and Needs R J 2010 *Nature Mater.* **9** 624
[3] Kolmogorov A N and Curtarolo S 2006 *Phys. Rev. B* **74** 224507
[4] Feng J, Hennig R G, Ashcroft N W and Hoffmann R 2008 *Nature* **451** 445
[5] Li X X, Tao X M, Chen H M, Ouyang Y F and Du Y 2013 *Chin. Phys. B* **22** 026201
[6] Yu B H and Chen D 2012 *Chin. Phys. B* **21** 060508
[7] Liang H N, Ma C L, Du F, Cui Q L and Zou G T 2013 *Chin. Phys. B* **22** 016103
[8] Ji X H, Zhang Q Y, Xu J Q and Zhao Y M 2011 *Prog. Solid State Chem.* **39** 51
[9] Xu Y, Zhang L, Cui T, Li Y, Xie Y, Yu W, Ma Y and Zou G 2007 *Phys. Rev. B* **76** 214103
[10] Young D P, Hall D, Torelli M E, Fisk Z, Sarrao J L, Thompson J D, Ott H R, Oseroff S B, Goodrich R G and Zysler R 1999 *Nature* **397** 412
[11] Kolmogorov A N, Shah S, Margine E R, Kleppe A K and Jephcoat A P 2012 *Phys. Rev. Lett.* **109** 075501
[12] Gonze X, Beuken J M, Caracas R, Detraux F, Fuchs M, Rignanese G M, Sindic L, Verstraete M, Zerah G, Jollet F, Torrent M, Roy A, Mikami M, Ghosez P, Raty J Y and Allan D C 2002 *Comput. Mater Sci.* **25** 478

[13] Perdew J P, Burke K and Ernzerhof M 1996 *Phys. Rev. Lett.* **77** 3865
[14] Hamann D R, Schlüter M and Chiang C 1979 *Phys. Rev. Lett.* **43** 1494
[15] Fuchs M and Scheffler M 1999 *Comput. Phys. Commun.* **119** 67
[16] Gajdos M, Hummer K, Kresse G, Furthmüller J and Bechstedt F 2006 *Phys. Rev. B* **73** 045112
[17] Perdew J P, Ruzsinszky A, Csonka G I, Vydrov O A, Scuseria G E, Constantin L A, Zhou X and Burke K 2008 *Phys. Rev. Lett.* **100** 136406
[18] Perdew J P and Wang Y 1992 *Phys. Rev. B* **45** 13244
[19] Zhong J L, Smith M E, Sowrey F E and Newport R J 2004 *Phys. Rev. B* **69** 224107
[20] Bader R F 1994 *Atoms in Molecules: A Quantum Theory* (Oxford: Oxford University Press)
[21] Henkelman G, Arnaldsson A and Jónsson H 2006 *Comput. Mater. Sci.* **36** 354
[22] Bork N, Bonanos N, Rossmeisl J and Vegge T 2011 *J. Appl. Phys.* **109** 033702
[23] Zhang R F, Legut D, Lin Z J, Zhao Y S, Mao H K and Veprek S 2012 *Phys. Rev. Lett.* **108** 255502
[24] Kimura S, Nanba T, Tomikawa M, Kunii S and Kasuya T 1992 *Phys. Rev. B* **46** 12196
[25] Qian S L and Qiao J 2003 *The Journal of Physical Chemistry A* **107** 7869
[26] Kimura S, Nanba T, Kunii S and Kasuya T 1994 *Phys. Rev. B* **50** 1406
[27] He X K, Zeng L B, Wu Q S, Zhang L Y, Zhu K and Liu Y L 2012 *Chin. Phys. B* **21** 067801
[28] Born M and Huang K 1998 *Dynamical Theory of Crystal Lattices* (Oxford: Oxford University Press)
[29] Wang J J, Meng F Y, Ma X Q, Xu M X and Chen L Q 2010 *J. Appl. Phys.* **108** 034107
[30] Voigt W 1928 *Lehrburch der Kristallphys* (Leipzig: Teubner Press)
[31] Reuss A and Angew Z 1929 *Math. Mech.* **9** 49
[32] Hill R 1952 *Proc. Phys. Soc. Lond.* **65** 349
[33] Ding Y C, Chen M, Gao X Y and Jiang M H 2012 *Chin. Phys. B* **21** 067101
[34] Xu X W, Hu L, Yu X, Lu Z M, Fan Y, Li Y X and Tang C C 2011 *Chin. Phys. B* **20** 126201
[35] Havva B O, Kemal C, Engin D and Haci O 2012 *Chin. Phys. B* **21** 047101
[36] Hao X, Xu Y, Wu Z, Zhou D, Liu X, Cao X and Meng J 2006 *Phys. Rev. B* **74** 224112
[37] Kanoun M B, Goumri-Said S and Reshak A H 2009 *Comput. Mater. Sci.* **47** 491
[38] Nieto-Sanz D, Loubeyre P, Crichton W and Mezouar M 2004 *Phys. Rev. B* **70** 214108
[39] Hu Z G, Yoshimura M, Mori Y and Sasaki T 2004 *J. Cryst. Growth* **260** 287
[40] Pugh S F 1954 *Philos. Mag.* **45** 823
[41] Shein I R and Ivanovskii A L 2008 *J. Phys.: Condens. Matter* **20** 415218
[42] Mattesini M, Ahuja R and Johansson B 2003 *Phys. Rev. B* **68** 184108
[43] Zhang R F, Veprek S and Argon A S 2007 *Appl. Phys. Lett.* **91** 201914
[44] Frantsevich I N, Voronov F F and Bokuta S A 1982 *Elastic Constants and Elastic Moduli of Metals and Insulators Handbook* (Kiev: Naukova Dumka)
[45] Bouhemadou A, Khenata R and Binomran S 2011 *Physica B* **406** 2851
[46] Kim K Y, Bretz K C, Every A G and Sachse W G 1996 *J. Appl. Phys.* **79** 1857
[47] Zhou Q, Zhang S and Lü Y 2001 *Mater. Sci. Eng. B* **83** 239
[48] Najafi S K, Bucur V and Ebrahimic G 2005 *Mater. Lett.* **59** 2035
[49] Pantea C, Stroe I, Ledbetter H, Betts J B, Zhao Y, Daemen L L, Cynn H and Migliori A 2009 *Phys. Rev. B* **80** 024112
[50] Auld B A 1973 *Acoustic Fields and Waves in Solids* Vol. I (New York: John Wiley & Sons Press)